Acta Geotechnica (2011) 6:195–203
DOI 10.1007/s11440-011-0146-3

RESEARCH PAPER

3D-electrical resistivity tomography monitoring of salt transport in homogeneous and layered soil samples

Cesare Comina · Renato Maria Cosentini · Gabriele Della Vecchia · Sebastiano Foti · Guido Musso

Received: 2 February 2011 / Accepted: 21 September 2011 / Published online: 11 November 2011

Abstract Monitoring transport of dissolved substances in soil deposits is particularly relevant where safety is concerned, as in the case of geo-environmental barriers. Geophysical methods are very appealing, since they cover a wide domain, localising possible preferential flow paths and providing reliable links between geophysical quantities and hydrological variables. This paper describes a 3D laboratory application of electrical resistivity tomography (ERT) used to monitor solute transport processes. Dissolution and transport tests on both homogeneous and heterogeneous samples were conducted in an instrumented oedometer cell. ERT was used to create maps of electrical conductivity of the monitored domain at different time intervals and to estimate concentration variations within the interstitial fluid. Comparisons with finite element simulations of the transport processes were performed to check the consistency of the results. Tests confirmed that the technique can monitor salt transport, infer the hydrochemical behaviour of heterogeneous geomaterials and evaluate the performances of clay barriers.

C. Comina
Dipartimento di Scienze della Terra, Università degli Studi di Torino, Turin, Italy
e-mail: cesare.comina@unito.it

R. M. Cosentini · G. Della Vecchia · S. Foti · G. Musso (✉)
Dipartimento di Ingegneria Strutturale e Geotecnica, Politecnico di Torino, Corso Duca degli Abruzzi, 24, 10129 Turin, Italy
e-mail: guido.musso@polito.it

R. M. Cosentini
e-mail: renato.cosentini@polito.it

G. Della Vecchia
e-mail: gabriele.dellavecchia@polito.it

S. Foti
e-mail: sebastiano.foti@polito.it

Keywords Advection · Clay barriers · Diffusion · Electrical resistivity · Monitoring · Soil laboratory testing · Tomography · Transport

1 Introduction and background

The study of transport of dissolved species through natural soils and manmade earth structures is complicated by different phenomena. For example, flaws in environmental barriers made of compacted clays or geosynthetic clay liners (GCL) can cause preferential flow paths for contaminants. Monitoring is then required to track contaminant transport, to locate potential dangerous leakages and to calibrate numerical models through back-analysis.

Direct monitoring through local concentration measurements, e.g. in the laboratory to draw breakthrough curves (e.g. [26]) or in situ through periodic sampling of pore fluid within wells (e.g. [12]), typically concerns a limited number of points in space and time. In situ, additional uncertainties are related to water mixing within the wells and disturbance of soil structure due to probe installation.

Imaging techniques can provide two- or three-dimensional representations of the investigated soil volume at different times. Being non-invasive, they do not disturb flow patterns and soil structure. Electrical resistivity tomography (ERT) allows the distribution of the electrical conductivity of an investigated domain to be inferred. With respect to other techniques, ERT has two main advantages: cost effectiveness and suitability for a wide range of scales, both in the laboratory and in situ. Moreover, electrical conductivity can be related to hydrological variables (water content, porosity, solute concentration) on the basis of both empirical and theoretical relationships (for a review see e.g. [25]). In situ measurements have been adopted in

geophysical prospecting to monitor contaminant flow (e.g. [22, 23]), showing the complexity of diffusion processes due to the variability of flow and transport in natural environments [18].

Laboratory applications of ERT have the strong advantage that tests can be performed under known boundary conditions and controlled soil properties so that a direct comparison with numerical simulations is possible. Laboratory experiences have documented the application of 2D ERT to monitor saline diffusion in reconstituted sand samples [7, 11] and in an undisturbed soil column [5]. In these experiments, electrical measurements were taken on horizontal planes and information on the 3D diffusion process was therefore limited. Koestel et al. [20] monitored transport of a tracer, applied as a uniform front, along a soil column through measurements taken by rings of electrodes placed at different heights; 3D inversions of such measurements provided excellent data concerning the migration of solute.

The present work evaluates the capabilities of 3D ERT in monitoring transport of a saline tracer originating from a punctual source. Tests to investigate solute transport in homogeneous and heterogeneous samples were performed in an oedometer cell (EIT oedometer), which allows spatial and temporal monitoring of electrical and seismic properties under controlled mechanical and hydraulic conditions [8]. The same equipment has been used to monitor transient flow events in the unsaturated range (back-analysis of these results allowed Cosentini et al. [10] deriving the water retention properties of non-plastic soil samples).

The cell has an internal diameter of 130 mm, and it can host samples with maximum height of 60 mm: 42 electrodes are placed on the internal boundary of the cell, 16 equally spaced on the sidewall and 13 on both the top cap and the base. A picture of the cell is reported in Fig. 1. Conductivity measurements for tomography require the injection of current at two electrodes, while other pairs of electrodes measure the induced electrical potentials. Different measuring quadruples must be used in order to investigate the conductivity distribution in the whole sample. In the present study, about 800 measurements were performed for each tomography (see [8]), for details about the measurement protocol). Differently from the scheme adopted by Koestel et al. [20], measurements are taken not only along the lateral side of the sample, but also vertically, particularly in the centre of the sample where the resolution of the inverse problem is poor. All the measurements are then used to reconstruct the electrical conductivity field within the sample, using an inversion technique based on a least-squares algorithm with Tikhonov regularisation. The soil is modelled with a finite element mesh, and the electrical conductivity of each element is estimated in order to obtain the final reconstruction [6]. Acquisition of a single set of measurements can be performed in a few minutes.

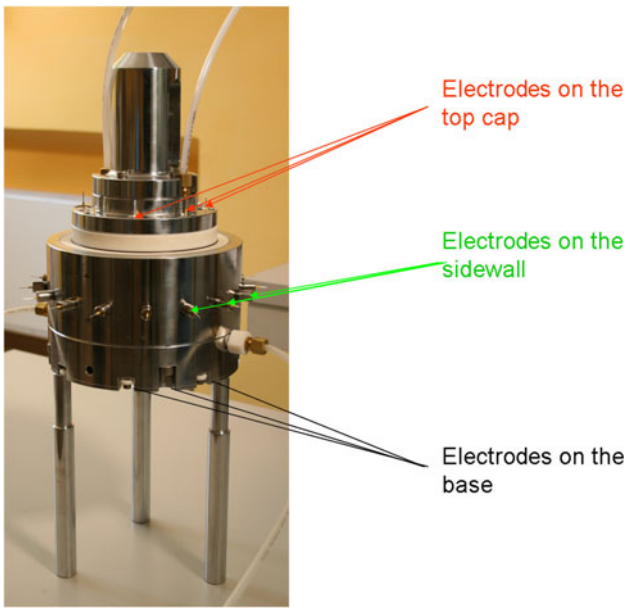

Fig. 1 Picture of the EIT-oedometer cell

2 Dissolution and transport tests

Tests have been performed to monitor solute transport in both homogeneous (Test 1) and heterogeneous (Tests 2 and 3) samples (Fig. 2). Few grams of NaCl were placed at a location on the top of the specimen (Fig. 2a). Salt grains were then submerged with distilled water to induce dissolution and subsequent diffusion towards the specimen. Electrical measurements were carried out for 3 days, approximately every 30 min, to monitor the movement of the solute. In all the tests, the measured average electrical conductivity of the sample increased during approximately the first 400 min and then remained constant. This time interval is likely related to the complete dissolution of the NaCl grains, whose rate is anyway controlled by the associated transport mechanism (see [2]). Measurements at

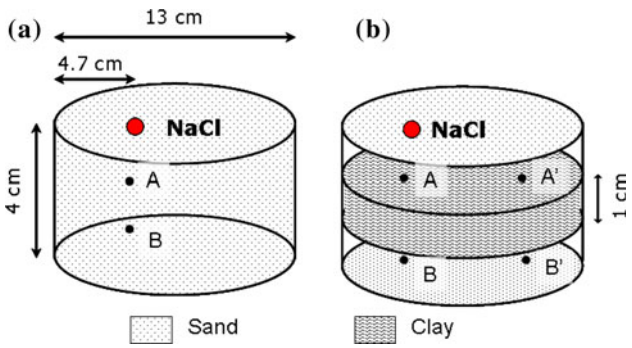

Fig. 2 Experimental set-up for the dissolution and transport tests: **a** homogeneous sample (Test 1), **b** heterogeneous sample (Tests 2 and 3)

subsequent times can then be associated with solute redistribution within the specimen, occurring at a constant global amount of salt.

The geometry of the experiment could lead to unstable flow conditions and to fingering, due to the fact that the denser miscible fluid (saline water) is initially above the lighter one. The adequateness of electrical techniques in general, and ERT in particular, to detect viscous and saline fingering has been documented in the literature (see e.g. [17, 27]).

2.1 Homogeneous sand specimens

Test 1 was performed on a homogeneous saturated specimen of Ticino Sand (Fig. 2a), a mono-granular siliceous sand with well-rounded particles with average size of 0.5 mm. The sample was prepared by moist-tamping at porosity $\phi = 0.40$. The height of the sample was 4 cm.

Since neither porosity nor degree of saturation changed during the test, the measured variations of the local electrical conductivity can be directly related to local variations of water salinity. The initial electrical conductivity of the pore fluid, measured with a conductimeter, was $\sigma_{w0} = 1.76$ mS/cm. The initial average electrical conductivity of the sample, as given by a tomographic reconstruction, was $\sigma_0 = 0.35$ mS/cm.

In Fig. 3, reconstructions taken during the first 90 min of testing are reported. The images show the elements of the mesh whose conductivity exceeded a threshold value of 2 mS/cm. They are representative of the volume experiencing an increase in solute concentration at different times. Images indicate that the solute was spreading with an almost hemispherical pattern, consistently with the homogeneity of the sample.

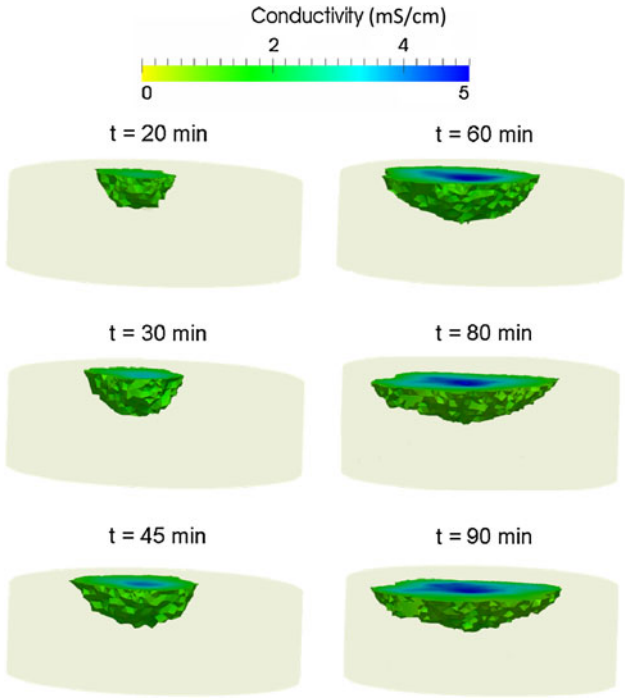

Fig. 3 3D diffusion test on homogeneous sand sample (Test 1): images of the solute plume at different times

2.2 Layered sand–clay specimens

Two tests were performed on layered specimens, prepared by placing between two layers of Ticino sand a 1-cm-thick clay layer (Fig. 2b) of reconstituted Spes White China Clay Kaolinite (Test 2) or of reconstituted Scanzano Clay (Test 3). The Spes White China Clay has liquid limit $w_L = 50\%$, plasticity index PI = 23% and activity $A = 0.28$. Scanzano clay is a natural illitic-kaolinitic clay, having liquid limit $w_L = 58\%$, plasticity index PI = 30% and activity $A = 0.88$. Samples were reconstituted in a consolidometer under a vertical effective pressure of 100 kPa; the main parameters characterising the hydro-electrical behaviour of the clay specimens in the conditions at which they were prepared and used in the tests are reported in Table 1 (data from [1, 9, 21]).

A sequence of reconstructed images for Test 2 is reported in Fig. 4. Salt appears to spread more in the horizontal direction than in the vertical one. The conductivity increase on the left flank of the specimen, appearing 45 min after test beginning, suggests that leakage occurred at the interface between the kaolin and the cell. Leakage was probably due to a weak contact between the soil and the cell wall, which could be linked to both the initial integrity of the kaolin layer and the shrinkage of the clay caused by chemical consolidation. As a consequence, the saline solute entered the bottom sand layer at first from the sidewall of the specimen ($t > 45$ min), while the clay layer is interested by transport occurring within the matrix only after 80 min. Salt percolation along the boundaries of the clay layer was observed during Test 3 as well.

Despite leakage, globally the clay layers appear to confine and retard the progress of dissolved NaCl. This effect can be observed by comparing the 3D reconstructions of the three tests at the same time $t = 90$ min (Fig. 5).

Table 1 Hydro-electrical characteristics of the clay specimens used for the tests

	Kaolin	Scanzano clay
Porosity, n (–)	0.5	0.49
Hydraulic conductivity, K_w (m/s)	4×10^{-9}	3.6×10^{-10}
Electrical conductivity, σ (S/m)	0.10	0.23
Archie's porosity exponent, m (–)	2.00	1.91
Electroosmotic conductivity, K_{eo} (m^2/Vs)	8×10^{-9}	2×10^{-9}

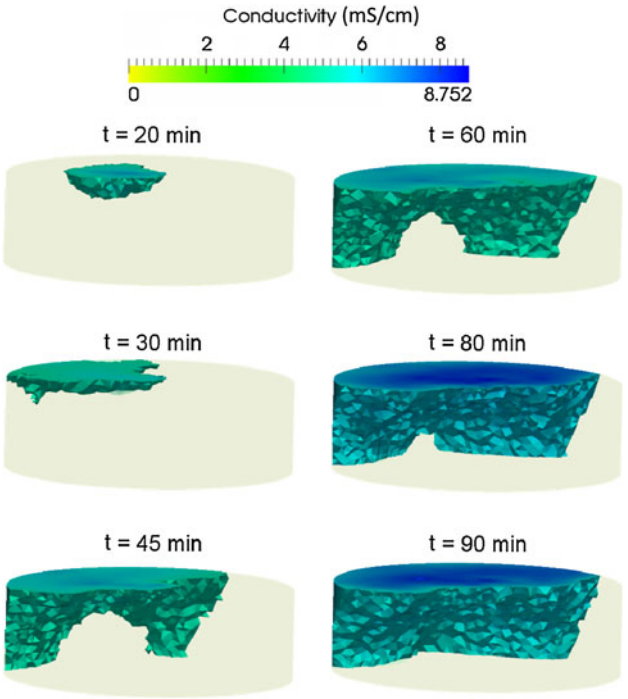

Fig. 4 3D diffusion test on layered sample (Test 2): images of the solute plume at different times

The flattening of the saline front for Test 2 and 3 (Fig. 5b, c) with respect to the test on the homogeneous sample (Fig. 5a) is evident. The contention effect provided by the barriers is also shown in Fig. 6, where images of horizontal sections of the specimens above the barrier (2.5 cm from the bottom of the sample) are reported at two different times. A very clear difference in terms of conductivity in the top layer is observed between the homogeneous and two layered samples.

3 Discussion and numerical validation of the tests

The reconstructed electrical conductivity distributions were compared to the results of numerical simulations referring to a homogenous and to a layered sample, to validate tomography results and to assist in understanding physical processes.

In the following, the terminology presented in Bear and Cheng [4] is used: the term "advection" is used to indicate the component of solute movement attributed to transport by the flowing water, while "transport" is used to indicate the sum of advection, diffusion and dispersion. Numerical simulations were performed by a finite element integration of the mass balance equations for the aqueous solution and for the solute. The effect of advection induced by density difference between dense aqueous solution and pure water was considered, consistently with the evidence presented

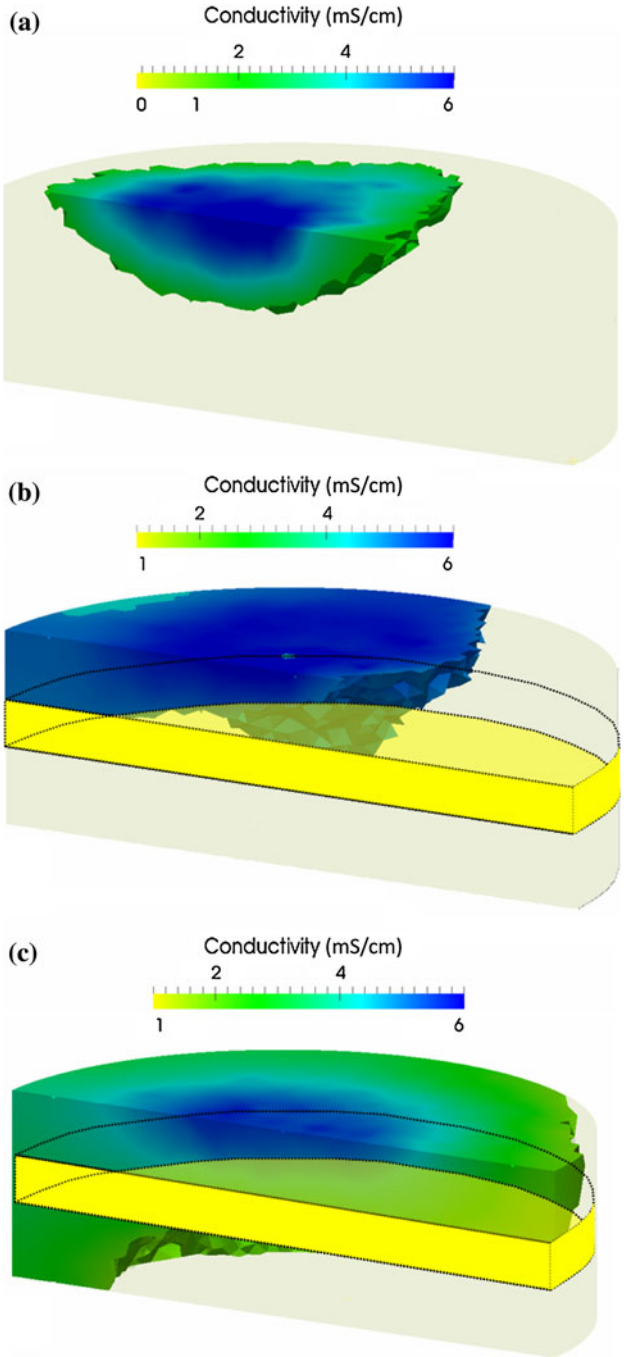

Fig. 5 Images of the solute plume at time $t = 90$ min from the beginning of the test: **a** Test 1; **b** Test 2; **c** Test 3

by Kirino et al. [19]. Density coupling of these equations is also accounted for as proposed by Huyakorn et al. [16] and Hassanizadeh and Leijnse [13].

The finite element solution of the coupled transient problem, determined in terms of the nodal values of concentration and water pressure, was obtained with commercial software (Comsol Multiphysics®). The domain was discretised into tetrahedral elements of eight nodes and the

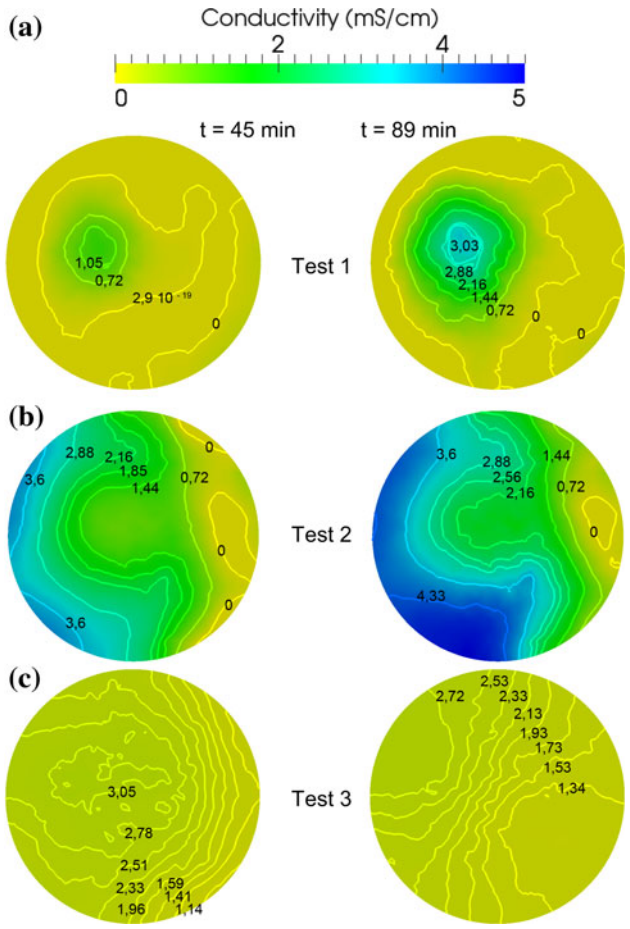

Fig. 6 Reconstructed electrical conductivity along horizontal sections at 2.5 cm from the base of the samples ($t = 45$ min and $t = 90$ min from the beginning of the diffusion): **a** Test 1; **b** Test 2; **c** Test 3

mesh was refined near the salt injection point. The adequateness of Comsol to simulate possible fingering phenomena has been pointed out by Holzbecher [14, 15].

Assuming no chemical reactions and constant porosity and degree of saturation, the mass balance equation of the solute can be written as (e.g. [4]):

$$\phi R_d \frac{\partial c}{\partial t} + c\nabla \cdot \mathbf{q} + \mathbf{q} \cdot \nabla c - \phi D \nabla^2 c = 0, \tag{1}$$

where ϕ = porosity, c = solute concentration, $\mathbf{q}$ = specific discharge, D = coefficient of hydrodynamic dispersion (sum of diffusion and mechanical dispersion) and R_d is the retardation factor accounting for the mass of solute adsorbed onto the solid grains.

The specific discharge, accounting for density variation, is given by the equation:

$$\mathbf{q} = -K\left(\nabla h_0 + \left(\frac{\rho - \rho_0}{\rho_0}\right)\nabla z\right). \tag{2}$$

The reference head h_0 is a function of the pore water pressure p, the vertical Cartesian coordinate z and pure water density ρ_0:

$$h_0 = z + \frac{p}{\rho_0 g}. \tag{3}$$

A parameter a is introduced to describe the evolution of water density with concentration, assumed linear as a first approximation:

$$\rho = \rho_0 + ac. \tag{4}$$

The mass balance for the water can be written as:

$$S_s \frac{\partial h_0}{\partial t} + \phi \frac{a}{\rho_0}\frac{\partial c}{\partial t} + \nabla \cdot (\mathbf{q}) = 0, \tag{5}$$

where S_s is the specific storage.

The whole boundary of the specimen was assumed impermeable to fluxes, except for the salt injection zone where a constant saline concentration, equal to the water solubility of NaCl (359 g/l), was imposed for times smaller than those of complete dissolution. Afterwards, impermeability to salt was assumed. Over this surface, the atmospheric pressure was imposed to the aqueous phase along the whole simulation.

The electrical conductivity of the interstitial water σ_w was related to c by relating the specific conductivity of the NaCl solution to salt concentration [24]. Given the initial water electrical conductivity, the initial salt concentration was estimated to be $c_{\text{init}} = 0.76$ g/l.

Archie's law [3] was then used to link the electrical conductivity of the soil with porosity and electrical conductivity of the pore fluid:

$$\sigma = \sigma_w \phi^m. \tag{6}$$

The fitting parameter m, calculated on the basis of the initial values of σ, σ_w and ϕ, was imposed equal to $m = 1.76$ for the sand and $m = 2.0$ for the clay, consistently with the measured values given in Table 1. The hydraulic conductivity of the clay layer was set as an intermediate value between the one of the two clay samples used in the tests. The complete set of parameters used in the simulations is reported in Table 2.

Table 2 Parameters used in the numerical simulations

Sand				Clay				ρ_0 (kg/m^3)	a (–)
ϕ (–)	K (m/s)	D/Rd (m^2/s)	m (–)	ϕ (–)	K (m/s)	D/Rd (m^2/s)	m (–)		
0.4	1×10^{-6}	3×10^{-10}	1.8	0.5	1×10^{-9}	6×10^{-11}	2.0	9.96×10^2	0.820

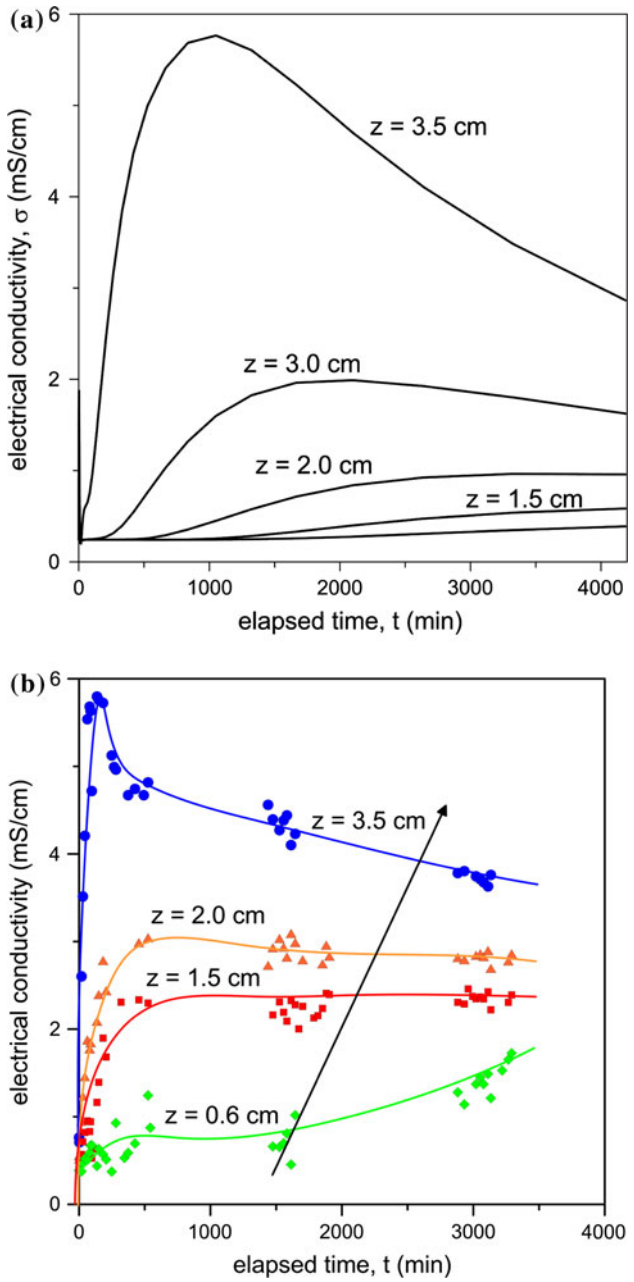

Fig. 7 Electrical conductivity breakthrough curves for the homogeneous sample at different heights along the *vertical line* passing through the NaCl source: **a** numerical simulation; **b** experimental data from ERT reconstructions of Test 1

It was here assumed that mechanical dispersion is limited, so that the diffusion coefficient adopted for the sand is $D = 3 \times 10^{-10}$ m^2/s, in line with literature data (e.g. [12]). It was as well assumed that the amount of salt adsorbed onto the sand particles is negligible, so that $R_d = 1$. The trend extracted from the simulation of the physical process (Fig. 7a) in the homogeneous sample condition is consistent with experimental observations (Fig. 7b). Close to the saline source, a peak of the electrical conductivity is recognised. During the homogenisation stage, electrical conductivity decreases with a trend towards a common asymptotic value. Both the reconstruction and the simulation predict the absence of the peak for z lower than 1.5 cm. Fig. 7b shows the experimental values from the ERT reconstructions, and a line is depicted to guide the reader to appreciate the evolution.

For the simulations of Test 2 and 3, the presence of an ideal confining barrier has been simulated. To take into account the adsorption phenomena in clayey soils, the apparent diffusion coefficient D/R_d was assumed as 1/5 of the sand diffusion coefficient, in line with literature data [26]. The simulated clay layer was assumed to be sealed to the cell wall, without allowing any leakage of solute at the interface.

Results obtained with the numerical simulation for two points located in the top and bottom sand layers (points A and B in Fig. 2a, b) are reported in Fig. 8 (dotted lines) and compared with the corresponding points for the homogeneous sample (continuous lines). Since the clay layer is expected to retard the migration of the solute, the model predicts that its presence would cause concentration in point A to increase faster (Fig. 8a) and concentration in point B to increase slower than the homogeneous case (Fig. 8b).

ERT reconstructions referring to the same points are presented in Fig. 9. As for point A, the experimental results are qualitatively in good agreement with model predictions (Fig. 9a), with Test 2 returning higher concentrations than Test 1. Nevertheless, retardation does not appear evident in point B, probably because of the clay barrier leakage (Fig. 9b).

To clarify this effect, Fig. 10 reports experimental conductivity values in two points on the other side of the cell (points A′ and B′ in Fig. 2b). The barrier effect provided by the clay layer is in this location appreciable also for the lower point (B′, Fig. 10b), where Test 2 shows a lower concentration than Test 1 for $t < 600$ min. Afterwards, conductivity increases faster in Test 2 than in Test 1, probably because of the leakage identified on the other side of the cell.

The overall behaviour of both the homogeneous and the layered samples was then checked by analysing the evolution of the dissolved salt mass in the pore fluid. This was evaluated by inverting Eq. 6, to infer the local values of σ_w from ERT reconstructions, and then by relating σ_w to the NaCl concentration c.

The mass of salt contained in a given volume of soil is then given by volume integration:

$$m = \int c\phi \mathrm{d}V \cong \sum_{i=1}^{n} c_i \cdot \phi_i \cdot \Delta V_i, \tag{7}$$

where c_i is the local estimation of the NaCl concentration, n the number of elements of the ERT mesh, ΔV_i the volume of the ith element and ϕ the porosity.

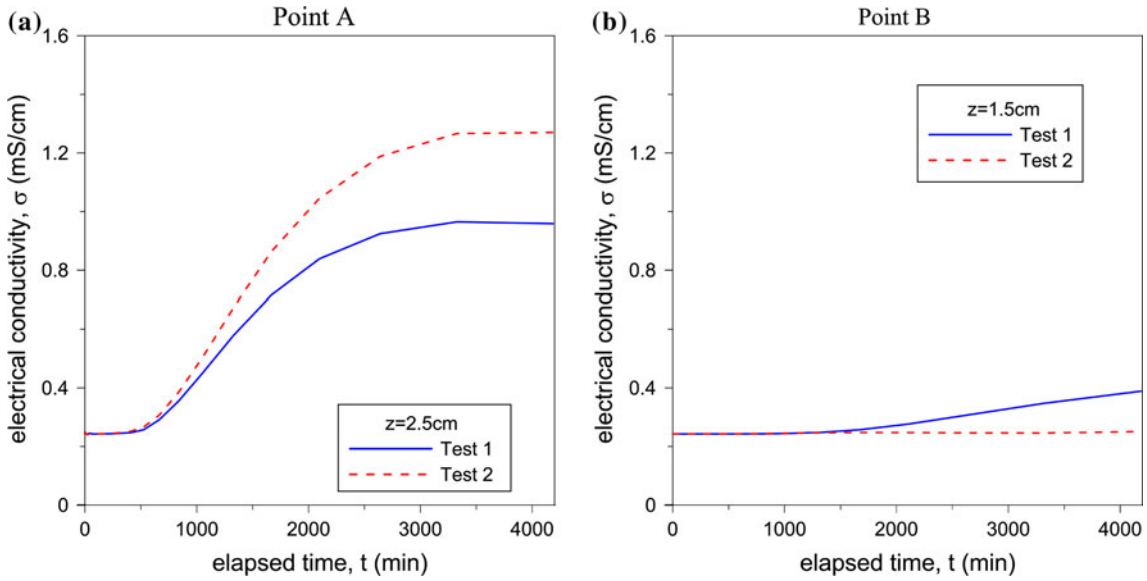

Fig. 8 Comparison of electrical conductivity breakthrough curves at point A and B (Fig. 2) predicted by the numerical simulation for the homogeneous sample and for the ideal (perfect contact) layered sample. The retardation effect provided by the clay layer can be appreciated for both points

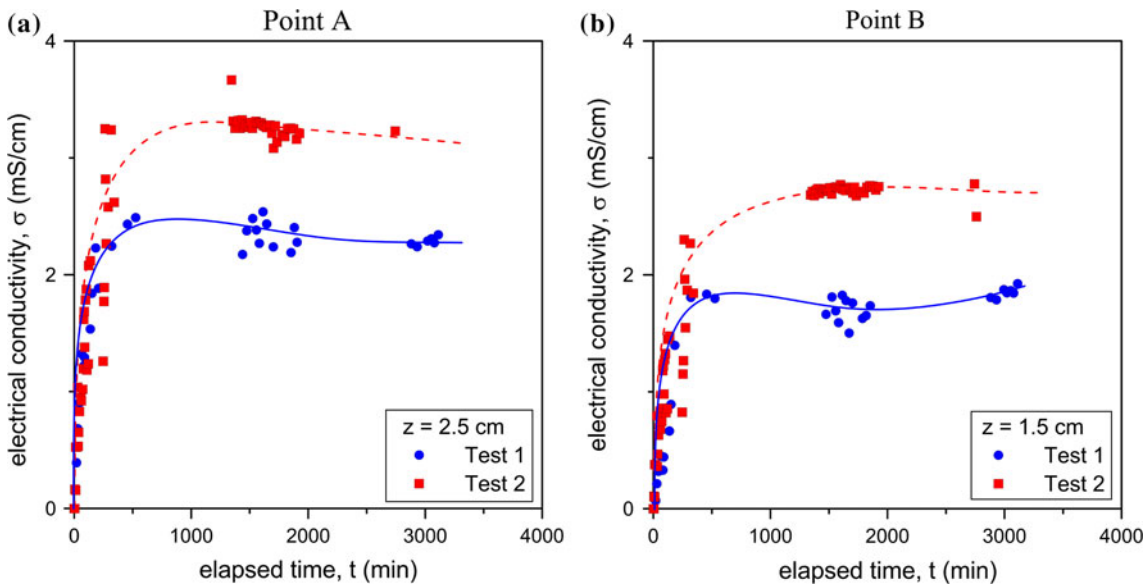

Fig. 9 Comparison of electrical conductivity breakthrough curves at point A and B (Fig. 2) as given by ERT reconstructions for Test 1 and Test 2. The consequences of leakage during Test 2 can be appreciated especially for point B

The time evolution of the salt mass contained in the upper portion of sand (lying over the clay, or in analogous position for Test 1), and that contained in the bottom one, is drawn in Fig. 11. Values are normalised with respect to the total mass of salt that entered the sample during the whole test. The good qualitative agreement between the simulations and the ERT reconstructions further suggests that the amount of salt that leaked was limited.

4 Conclusions

Most situations in which monitoring the transport of ionic substances is of critical importance involve three-dimensional geometries, due to punctual sources of contamination and soil heterogeneities. The tests presented in this paper were designed to check the capabilities of 3D ERT in investigating transport of contaminants, under well controlled boundary conditions.

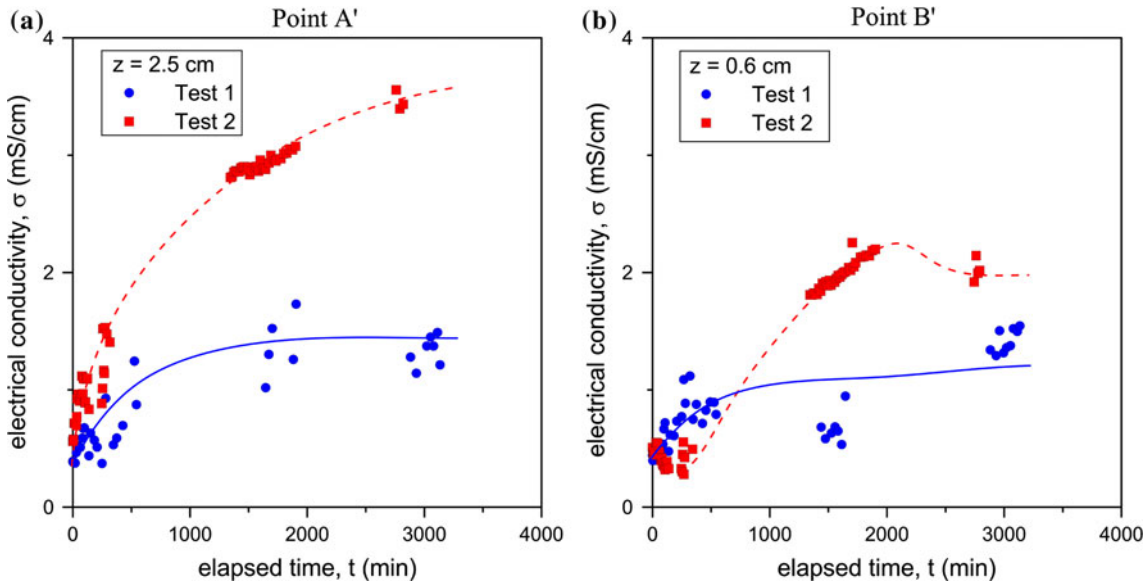

Fig. 10 Electrical conductivity breakthrough curves at point A′ and B′ (Fig. 2) as given by ERT reconstructions for Test 1 and Test 2

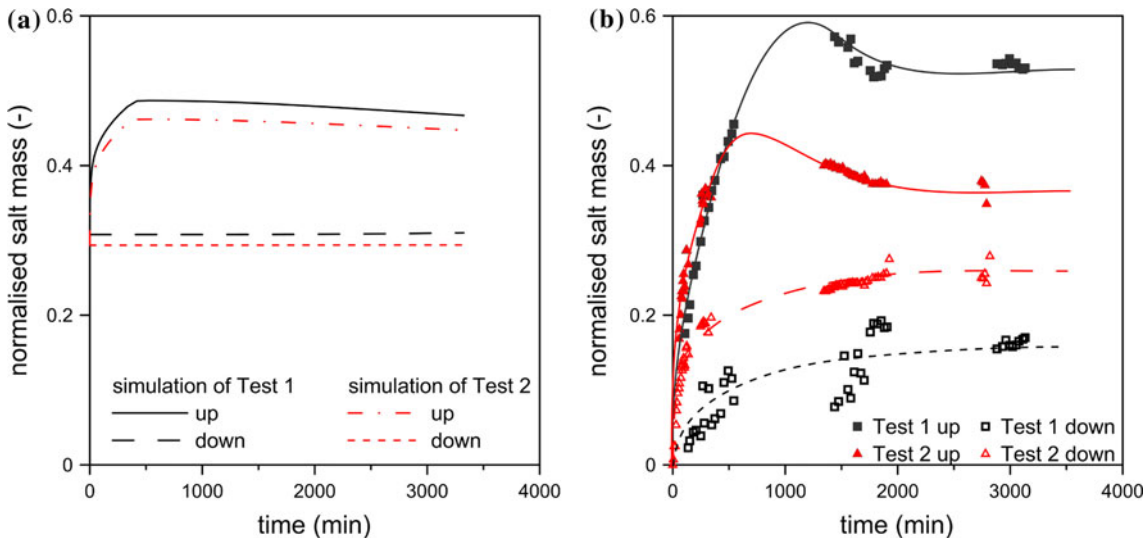

Fig. 11 Evolution with time of normalised salt mass distribution in Test 1 and Test 2: **a** numerical simulations; **b** ERT reconstructions

ERT located the position of the salt source and reconstructed the shape of the solute plume for both homogeneous and heterogeneous samples. Test results, interpreted in terms of evolution of local electrical conductivity, highlighted leakage due to weak contact between the clay barrier and the cell wall. The detection of these leakages shows the potentiality of 3D ERT in reconstructing complex diffusive flows and preferential flow paths. By integrating electrical conductivity over the volume of the different soil layers, the amount of transport occurring across this preferential flow path was however found to be relatively modest.

Numerical simulations of a homogeneous sample and of a layered sample provided an assessment of the consistency of the tomographic reconstruction. Further research developments will concentrate on the possibility of using some of the information provided by ERT monitoring as a supporting tool for the calibration and validation of numerical models, possibly leading to a further integration of ERT measurements into procedures of parameter estimation.

Acknowledgments The present work has been partially supported by the research project SoilCam funded by the EU Commission 7th FP and by the Italian National Research Project PRIN 2008B5T829_004.

References

1. Airoldi F, Jommi C, Musso G, Paglino E (2009) Influence of calcite on the electrokinetic treatment of a natural clay. J Appl Electrochem 39(11):2227–2237
2. Appelo CAJ, Postma D (1993) Geochemistry, groundwater and pollution. Balkema, Rotterdam
3. Archie GE (1942) The electrical resistivity log as an aid to determining some reservoir characteristics. Trans AIME 146: 54–63
4. Bear J, Cheng AHD (2009) Modeling groundwater flow and contaminant transport. Springer, New York
5. Binley A, Henry-Poulter S, Shaw B (1996) Examination of solute transport in an undisturbed soil column using electrical resistance tomography. Water Resour Res 32(4):763–769
6. Borsic A, Comina C, Foti S, Lancellotta R, Musso G (2005) Imaging heterogeneities with electrical impedance tomography: laboratory results. Géotechnique 55(7):539–547
7. Comina C, Foti S, Lancellotta R, Musso G, Borsic A (2005) Imaging heterogeneities and diffusion in sand samples. In: Proceedings of the 11th international conference of the international association of computer methods and advances in geomechanics IACMAG. Torino, vol 2, pp 27–34
8. Comina C, Foti S, Musso G, Romero E (2008) EIT oedometer—an advanced cell to monitor spatial and time variability in soil. Geotech Test J ASTM 31(5):404–412
9. Comina C, Cosentini RM, Foti S, Musso G (2010) Electrical tomography as laboratory monitoring tool. Rivista Italiana di Geotecnica 44:15–26
10. Cosentini RM, Della Vecchia G, Foti S, Musso G (2012) Estimation of the hydraulic parameters of unsaturated samples by electrical resistivity tomography. Géotechnique. In print
11. Damasceno VM, Fratta D, Bosscher PJ (2009) Development and validation of a low-cost electrical tomographer for soil process monitoring. Can Geotech J 46:842–854
12. Freeze AR, Cherry JA (1979) Groundwater. Prentice Hall, Englewood Cliffs
13. Hassanizadeh SM, Leijnse T (1988) On the modelling of brine transport in porous media. Water Resour Res 24(3):321–330
14. Holzbecher E (2005) FEMLAB performance on 2D porous media variable density benchmarks. In: Proceedings of FEMLAB Konferenz, pp 203–208
15. Holzbecher E (2009) Modeling of viscous fingering. In: Proceedings of the 2009 COMSOL conference. Boston
16. Huyakorn PS, Andersen PF, Mercer JW, White HO (1987) Saltwater intrusion in aquifers: development and testing of a three dimensional finite element model. Water Resou Res 23(2): 293–312
17. Jiao CY, Holtz H (2004) An experimental study of miscible displacements in porous media with variation of fluid density and viscosity. Transp Porous Med 54:125–144
18. Kemna A, Vanderborght J, Kulessa B, Vereecken H (2002) Imaging and characterisation of subsurface solute transport using electrical resistivity tomography (ERT) and equivalent transport models. J Hydrol 267:125–146
19. Kirino Y, Yokoyama T, Hirono T, Nakajima T, Nakashima S (2009) Effect of density-driven flowon the through-diffusion experiment. J Contam Hydrol 106:166–172
20. Koestel J, Kemna A, Javaux M, Binley A, Vereecken H (2008) Quantitative imaging of solute transport in an unsaturated and undisturbed soil monolith with 3-D ERT and TDR. Water Resour Res 44(W12411). doi:10.1029/2007WR006755
21. Musso G (2000) Electrokinetic phenomena in soils. PhD Thesis, Politecnico di Torino
22. Müller K, Vanderborght J, Englert A, Kemna A, Huisman JA, Rings J, Vereecken H (2010) Imaging and characterization of solute transport during two tracer tests in a shallow aquifer using electrical resistivity tomography and multilevel groundwater samplers. Water Res Res 46(W03502). doi:10.1029/2008WR007595
23. Reynolds JM (1997) An introduction to applied environmental geophysics. Wiley, Chichester
24. Robinson RA, Stokes RH (1968) Electrolyte solutions. Butterworths, London
25. Santamarina JC in collaboration with Klein KA, Fam MA (2001) Soils and waves. Wiley, New York
26. Shackelford CD, Daniel ED (1991) Diffusion in saturated soil. I: background. J Geotech Eng 117(3):467–484
27. Van Dam RL, Simmons CT, Hyndman DW, Wood WW (2009) Natural free convection in porous media: first field documentation in groundwater. Geophys Res Lett 36(L11403). doi:10.1029/2008GL036906